Analytical and Bioanalytical Chemistry (2021) 413:3861–3872
https://doi.org/10.1007/s00216-021-03336-1

RESEARCH PAPER

Determination of minimal sequence for zearalenone aptamer by computational docking and application on an indirect competitive electrochemical aptasensor

Farah Asilah Azri[1] · Jinap Selamat[1,2] · Rashidah Sukor[1,2] · Nor Azah Yusof[3] · Nurul Hanun Ahmad Raston[4] · Shimaa Eissa[5] · Mohammed Zourob[5] · Raja Chinnappan[5]

Received: 26 February 2021 / Revised: 28 March 2021 / Accepted: 9 April 2021 / Published online: 21 May 2021

Abstract

Aptamers are short single-stranded oligonucleotides (either DNA or RNA) that can fold into well-defined three-dimensional (3D) spatial structures which enable them to capture their specific target by complementary shape interactions. Aptamers are selected from large random libraries through the SELEX process and only a small fraction of the sequence is involved in direct docking with the target. In this paper, we describe the possible truncation variants of zearalenone (ZEA) aptamer which might be an effective binding region for the target. The originally selected zearalenone (ZEA) aptamer was 80-mer in length and shown to bind the target with a high affinity ($K_d = 41 \pm 5$ nM). Herein, computational docking simulation was performed with 15 truncated variants to determine the predicted binding energy and responsible binding site of the aptamer-analyte complex. The results revealed that 5 truncated variants had binding energy lower than − 7.0 kcal/mol. Circular dichroism analysis was performed on the shortlisted aptamer and the conformational change of aptamers was observed with the presence of an analyte. Aptamer Z3IN (29-mer) was chosen as the most enhanced affinity for its target with a dissociation constant of 11.77 ± 1.44 nM. The aptamer was further applied in the electrochemical aptasensor of ZEA based on an indirect competitive format. The results demonstrated that the truncated aptamer leads to an enhancement of the sensitivity of the biosensor.

Keywords Aptamers · Computational docking · Truncation · Zearalenone

Introduction

Antibodies have been always considered the common biological component to detect the specific analyte in biosensor development. However, aptamers are the trending alternative of antibodies, especially for the detection of small molecules such as toxins, antibiotics, molecular markers, drugs, heavy metals, and ions [1]. Aptamers are single-stranded, synthetic oligonucleotides (DNA or RNA) that able to fold into 3-dimensional (3D) shapes and can bind non-covalently to the target molecule with high affinity [1]. Aptamers have been widely used in the diagnostics of various substances due to their inherent specificity and affinity. Numerous studies have been reported on the application of aptamers for the detection of mycotoxins, especially aflatoxin B_1 (AFB_1), ochratoxin A, and fumonisin B1 (OTA) [2–9]. However, limited studies can be found on zearalenone (ZEA) detection, especially via electrochemical transducing platform [10–13]. ZEA is an oestrogenic mycotoxin formed by several *Fusarium* species and commonly contaminates cereals used for food and animal feed. Besides estrogenic effects, ZEA may cause alterations in the reproductive tract of the animals, especially mice, rats, guinea pigs, rabbits, cattle, swine, and poultry, with pigs as the most sensitive animals [14].

✉ Jinap Selamat
sjinap@gmail.com; jinap@upm.edu.my

[1] Food Safety and Food Integrity, Institute of Tropical Agriculture and Food Security, Universiti Putra Malaysia, UPM, 43400 Serdang, Selangor, Malaysia

[2] Department of Food Science, Faculty of Food Science and Technology, Universiti Putra Malaysia, UPM, 43400 Serdang, Selangor, Malaysia

[3] Department of Chemistry, Faculty of Science, Universiti Putra Malaysia, UPM, 43400 Serdang, Selangor, Malaysia

[4] School of Bioscience and Biotechnology, Faculty of Science and Technology, Universiti Kebangsaan Malaysia, UKM, 43600 Bangi, Selangor, Malaysia

[5] Department of Chemistry, Alfaisal University, Al Zahrawi Street, Al Maather, AlTakhassusi, Riyadh 11533, Saudi Arabia

During SELEX process, constant region of primer binding site should be well designed to prevent primer-dimer pairs and self-priming during PCR amplification as well as to reduce the possibility of base pairing between the two constant regions [15]. These two constant regions are the forward and reverse priming regions that flanked the random nucleotides. However, it is not necessary that each nucleotide of the sequence needs to be involved in the target binding, providing that only the short part of full aptamer sequences is participating as the binding site [16]. This suggests that a short library, which is cost-effective and more comfortable to manage, can be employed for successful aptamer selection. But still, long random sequences in a library are more suitable in providing higher structural complexity, which is significant in isolating aptamers with high affinity and also increase the prospect for successful aptamer selection. That is why, the aptamers can then be further truncated as desired, by eliminating the fixed primer sequences as well as those identified not to be part of the consensus motif [17]. Several studies have revealed that it is crucial to minimise the length of the aptamer [16, 18]. Therefore, there is a need to study and determine the minimal sequence for binding of an aptamer, once produced by the SELEX process.

It is proven that truncation of an aptamer can improve the binding affinity as well as the performance [19]. Moreover, truncated aptamer may encourage better switching upon binding to the target that can be further employed in various detection assays [19]. The secondary structure information of aptamer can be predicted using computer simulation programs, giving guidance to the researcher on the conserved stem-loop regions, which are expected to be involved in target binding [20]. However, it cannot directly define at which position that the binding may take place within the full-length aptamer. Due to that reason, truncation trials at different regions of the full-length aptamer are required. Therefore, in this study, we employed a computational docking method to predict the truncated aptamers' efficiency.

Computational or molecular docking is generally achieved between a small molecule (ligand) that is flexible and a rigid macromolecule. The aims of the simulation are to understand the molecular recognition, discover the prominent and favourable binding side, predict the binding affinity of a ligand with the aptamer, and validate the ligand stability. This docking simulation method is very efficient for the screening of a large set of ligands and the refining of the structures of the final complexes [21]. Molecular docking associates a conformational search process and a scoring function to allocate the binding affinity for a ligand [22]. This scoring function can be empirical, force field-based, or knowledge-based. The molecular mechanics' energy and solvation models are essential in assessing the ligand-nucleic acid complex, as predicted by the docking program [23]. The predicted binding strength of the ligand is extracted from the docking trajectories [22]. This simulation approach disables the constraint in movement imposed on the aptamer and thus enabling for an induce fit in the ligand-nucleic acid binding [21].

Indirect competitive format detection is generally employed in detection of small molecules including ZEA, due to the main challenges related to limited binding site. Because of that, we report the development of an indirect competitive aptasensor using a label-free aptamer previously against ZEA [10]. In that report, the detection of ZEA was performed by immobilising the ZEA onto the gold electrode using cysteamine hydrochloride (Cys-HCl) and 1,4-phenylene diisocyanate (PDIC) linker. The free ZEA in the sample was allowed to compete with the immobilised ZEA for the binding site of fixed amount ZEA aptamer. Herein, the shortened aptamer is then integrated based on a similar assay. The truncation of the aptamer leads to increased affinity to their targets and enhanced the sensitivity of the aptasensor.

Materials and method

Reagents and chemicals

All routine reagents including ZEA ($C_{18}H_{22}O_5$), cysteamine hydrochloride (cys-HCl), 1,4-phenylene diisocyanate (PDIC) linker, N,N-dimethylformamide (DMF), acetonitrile (ACN), methanol (MeOH), potassium ferrocyanide ($K_4Fe(CN)_6$), potassium ferricyanide ($K_3Fe(CN)_6$), magnesium chloride ($MgCl_2$), sodium chloride (NaCl), tris-hydrochloride (Tris HCl), toluene, and sulphuric acid (H_2SO_4) were purchased from Sigma-Aldrich (St. Louis, MO, USA https://www.sigmaaldrich.com). Oligonucleotides were procured from Integrated DNA Technologies (IDT, Singapore) with the list of base sequences provided in Table S1 (see Supplementary Information, ESM). The aptamer and analyte solutions were prepared in binding buffer (50 mM Tris + 150 mM NaCl + 2 mM $MgCl_2$). The Cys-HCl and PDIC solution were prepared in ultrapure water and toluene, respectively. The redox solution of 5 mM $[Fe(CN)6]^{3-/4-}$ redox pair (1:1 M ratio) was prepared in 0.01 M phosphate-buffered saline, pH 7.4. Millipore Milli-Q ultrapure water (18.2 MΩ cm) was used in all experiments. All chemicals were of analytical grade and used without further purification.

Instrumentation

All electrochemical measurements were performed using Autolab PGSTAT302N potentiostat/galvanostat from Metrohm (Herisau, Switzerland, https://www.metrohm.com) connected to a computer operated by Nova 1.11 software. A three-electrode system was used for all electrochemical measurement consisting a gold working electrode, Ag/AgCl reference electrode (3M KCL), and Pt wire as the counter/

auxiliary electrode (Austin, Texas, USA, https://www.chinstruments.com/). Ten millilitres of the electrolyte $[Fe(CN)_6]^{3-/4-}$ redox pair was used in the electrochemical cell for each measurement. Circular dichroism (CD) measurements were done using Jasco-810 spectropolarimeter (Jasco, USA, https://www.jascoinc.com).

Protein search

The ZEA structure in PDB format for computational docking was obtained from Protein Data Bank (PDB ID: 5KRC) (https://www.rcsb.org/).

Truncation design of aptamer sequence

Several different truncation series of aptamer were studied to ascertain which part of the full aptamer sequence is essential for target binding. Fifteen truncated aptamers as provided in Table S1 (see ESM) were generated based on secondary structure of the full-length aptamer (8Z31). The secondary structure of the aptamer was predicted using free access Mfold software at http://www.unafold.org/mfold/applications/dna-folding-form.php (the RNA Institute, Albany, NY). The sequence was registered as FASTA format before proceeded with the folding. The truncated aptamers were designed by omitting different parts from the original aptamer structure, and new secondary structures were predicted.

Aptamer-ZEA computational docking

The PDB structure of ZEA was used as a ligand of the experimental object. This is due to smaller size compared to the aptamer. Meanwhile, the ZEA aptamer sequence was used as the receptor (macromolecule). The preparation of the receptor and ligand was done using AutoDock Tools, while the molecular docking was performed by AutoDock Vina, which is an open-source docking programme that is widely used for docking and virtual screening studies. In this study, the dot-bracket formats of Mfold output were used as input for the RNAComposer web server (http://rnacomposer.cs.put.poznan.pl/), for designing the three-dimensional structure of sequences. Since the output of RNAComposer is in RNA form, the three-dimensional structures of the RNA sequence were modified by changing the uracil bases to thymine bases manually using Microsoft Word. The PDB formats of ZEA and DNA sequence were used for molecular docking simulation via AutoDock Vina. The binding sites of aptamer and ZEA were studied using fully automated protein-ligand interaction profiler server (PLIP; https://projects.biotec.tu-dresden.de/plip-web/plip/index). The outputs of AutoDock Vina were visualised using PyMOL software.

Conformational evaluation of aptamer by circular dichroism

Circular dichroism (CD) spectroscopy was used to observe the conformational change of the aptamer in the presence of the analyte. The analysis was performed as described in our previously published article [10], using 1.0 μM ZEA aptamer in binding buffer, pH 7.4. The measurements were done in a 0.1-cm path length, quartz cuvette in an optical chamber. The chamber was purged with dry purified nitrogen gas (99.99%) prior to use and was kept in the nitrogen atmosphere along with the measurements. Each CD spectrum was scanned from 340 to 230 nm at 0.1 nm intervals, accumulation of three scans at 50 nm/min with a 1-nm bandwidth, and a time constant of 1 s.

Dissociation constant (K_d) determination of truncated aptamer using electrochemical impedance spectroscopy

The affinity of the aptamer towards ZEA was determined by performing a binding assay using a constant amount of ZEA (1000 ng/mL) immobilised on the electrode and various concentrations of the aptamer (0 to 250 nM). The immobilisation of ZEA on the electrode was done similarly, as described by Azri et al. (2020) [10] (see ESM). The measurements were done by electrochemical impedance spectroscopy (EIS). The measurements were recorded over a frequency range from 10 kHz to 1.0 Hz using an alternative voltage with an amplitude of 10 mV, superimposed on a DC potential of 0.20 V (vs. Ag/AgCl reference electrode). The measurements were performed in a 0.01 M PBS buffer solution containing 5 mM $[Fe(CN)_6]^{3-/4-}$ redox pair (1:1 M ratio). The saturation curve was obtained, and the dissociation constant (K_d) for the ZEA aptamer was calculated by one-site binding model using GraphPad Prism 5 software (San Diego, CA).

Electrochemical detection of ZEA using truncated aptamer

The zearalenone detection was done by a similar procedure described in our previous study [10]. The aptamer was first pre-treated by heating at 90 °C for 5 min, followed by cooling for 10 min at both 4 °C and room temperature. Then, 10 μL of the specific concentrations of free ZEA was pre-incubated with 50 nM of ZEA aptamer for 10 min at room temperature. The mixture was then transferred onto the immobilised Au/Cys/PDIC/ZEA electrode and incubated for another 35 min. The electrode was rinsed using 0.1 M Tris HCl prior to measurement. The electrochemical measurement was conducted using SWV, scanning from 0.45 to − 0.1 V at a scan rate of 0.125 V/s, with 0.02 V amplitude and frequency of 25 Hz. The

measurement was done in a 0.01 M PBS buffer solution containing 5 mM $[Fe(CN)_6]^{3-/4-}$ redox pair (1:1).

Results and discussion

Truncation design of aptamer sequences

The original 80-mer ZEA aptamer produced by SELEX was obtained from previous study with a reported dissociation constant (K_d) of 41 ± 5 nM [24]. The aptamer was further truncated by removing the reverse and forward primer sites, leaving a 40-mer ZEA aptamer. An indirect competitive electrochemical aptasensor using the 40-mer aptamer was successfully developed by our group [10]. Herein, this aptamer was further truncated into a shorter sequence. As it is known that only a particular section of the aptamer is critical for the binding target, hence, truncation of aptamer may lead to an improvement in aptamer binding [25]. Thus, as a first step to establish the structure-activity relationship of the ZEA aptamer towards its target, the ZEA aptamer sequence was subjected to Mfold software using the default DNA parameters. This analysis predicted the secondary structure of the ZEA aptamer, as shown in Fig. 1 with a minimum free energy of − 7.00 kcal/mol. This predicted secondary structure displayed that the ZEA aptamer contained two stem-loop-like forms. Therefore, to identify their independent role subjecting to which part was responsible for the binding, the parent aptamer was truncated into 15 guided variants (Z31A–Z31O). Aptamer Z31A is a similar 40-mer aptamer that had been used in previous study. This aptamer was included for a comparison with other truncated aptamers.

The truncation variants were primarily selected empirically, but it has also been described that predicted secondary structures can be used as guidance [16, 26]. The analyte-binding regions of an aptamer were often located in the stem and loop [27]. Besides, some linear parts could also be obligatory for supporting the binding between the aptamer and its target [19]. In this study, the truncation design was done by considering the three stem-loop-like sections, including (a) left-side hairpin loop, (b) right-side hairpin loop, and (c) multibranch loop (Fig. 1). A series of base changes were introduced within those three sections in an attempt to identify the sequence/structural elements necessary for binding to ZEA. This was due to changes in the full sequence of only one base would significantly alter the aptamer structure and affinity. Therefore, these changes were made to either preserve or disrupt these various structural elements [26]. The truncated aptamers were designed with lengths ranging from 13- to 46-mer. Inherent in these experiments is the assumption that the base changes only create local changes in the DNA aptamer structure and not a global change in folding [26]. Figures of the truncation designs of all 15 variants are provided in the ESM (Fig. S1), where the bases in red represent the new ssDNA sequence of the truncation was made.

The new truncated sequences were re-subjected into the Mfold software to obtain new secondary structures, as shown in Fig. 2. Based on the structures, almost all of them showed a hairpin structure with one or two loops and stems. A hairpin developed when a single strand DNA was folding back itself to form a helix capped at one end with a loop of single-stranded residues [28]. For this to occur, the DNA sequence must contain at least approximately a dyad symmetry. Analysis of the nucleotide contents showed that the pyrimidines (cytosine and thymine) were dominant in most of the loop structures. Truncated variants of Z31A, Z31D, Z31G, and Z31H were the most extended sequences among all fifteen candidates, which consisted of 40-mer, 46-mer, 36-mer, and 41-mer bases, respectively. These four variants were truncated by involving both left-side and right-side hairpin loop sections and subsequently have a similar trend of structure, which consisted of two hairpins. Meanwhile, Z31E and Z31F were variants derived from the left-side loop section, which consisted of 17- and 20-mer bases. Although these variants differed by a slight three bases, their secondary structures were seen to be different. Z31F has a new order of bases in the loop, while Z31E had a similar loop trend compared to the full-length aptamer structure.

To represent the right-side loop section, Z31B and Z31C were designed as 31- and 25-mer bases, respectively. Based on the secondary structure, the structure of these two variants was almost similar. Both variants consisted of similar shape and order of loop, with a different length of the stem. Based on the results of prediction binding affinity, it was assumed that the right-side hairpin loop might be responsible for the binding site. Hence, the aptamer was further truncated by focusing only on the right-side hairpin loop, including the stem. Z31I (13-mer) and Z31J (19-mer) were two variants representing the stem section. This was to ensure that the stem without loop was not obligated in the binding event. Meanwhile, Z31K, Z31L, Z31M, Z31N, and Z31O were five variants that were truncated by focusing on the right-side loop section. As shown in Fig. 2, all these new truncated aptamers have similar hairpin-like structure but only differed by their positions.

Table 1 provides the information on the lowest free energy ΔG (kcal/mol), which was obtained from the secondary structure predicted by the Mfold software. Based on the results, Z31E, Z31F, Z31I, and Z31J had high free energy values of 0.15, − 0.76, − 1.78, and − 1.78 kcal/mol, respectively. These variants were derived from the left-side loop section including stem section. From a thermodynamic perspective, the binding of the aptamer with its target comprising enthalpy (ΔH) and entropy (ΔS) changes could be defined by the change in free energy of binding (ΔG), the main driving force of the formation of the aptamer-target complex. Binding enthalpy reflected the energy change taking place when the aptamer binds to the

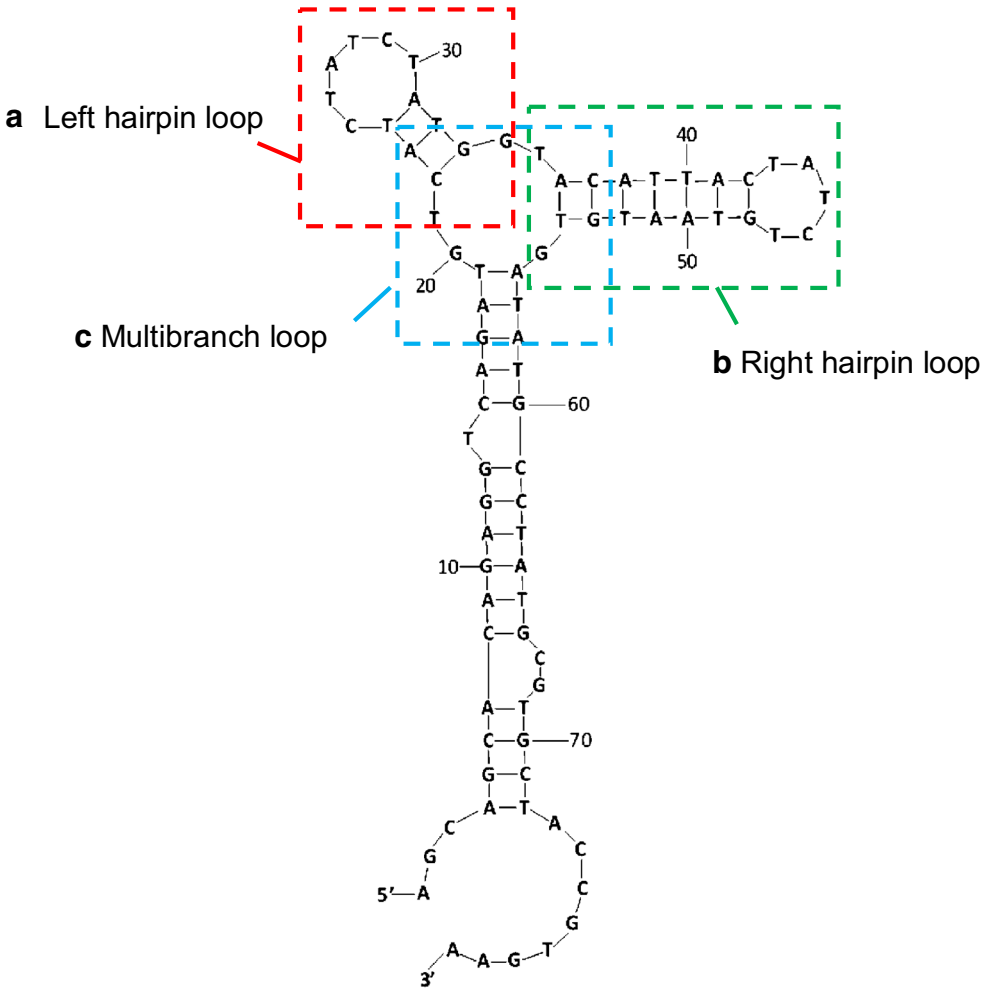

Fig. 1 Secondary structure of original Z31 aptamer as predicted by Mfold and three stem-loop sections involved in the truncation design

target; it was negative in the case of the exothermic process, implying the formation of energetically favourable non-covalent interactions between both aptamers [29]. Therefore, based on this basis, the right-side loop was assumed to contribute to the binding event. Furthermore, the free energy derived from the structure including the right-side loop was significantly lower, compared to the left-side variants.

Binding simulation by computational docking

After designing the 2D structure of the truncated aptamers, these aptamers were subjected to the RNA composer to obtain the 3D structure of the aptamer. However, it is worth noting that the sequence was changed to RNA structure by the software, and therefore, the uridine (U) nucleotide needs to be replaced manually back to thymines (T) for actual docking of DNA aptamer-ligand complex. The aptamer-ligand structure has primarily directed to the development of a variety of empirical scoring functions based on relatively simple descriptions of intermolecular interactions. The automated AutoDock Vina algorithm searched all possible interactions between the aptamer and ZEA based on atomic contact energies. This method was reported to be successful in ranking binding affinities when docked to a particular protein or in rather qualitative approximations of molecular fit in fast docking calculations [30]. It gives a score to each complex so that the better complex has a higher score. However, in terms of free binding energy, lower energy value represented a better and stable complex. This was relatable to the Gibbs free energy, where negative value showed that the ligand-bound spontaneously without consuming energy [31].

AutoDock Vina binding energy scores of the truncated aptamer-ZEA complexes are shown in Table 2. The free binding energy was calculated as:

$$\Delta G_{bind} = \Delta H – T\Delta S \quad (1)$$

where the ΔH represents the enthalpic, and $T\Delta S$ is the entropic contribution. Typically, if a ligand binds to a protein, the enthalpic term decreases due to favourable intermolecular interactions and the formation of intermolecular bonds. Based on the results, the binding energy value was slightly different from each other. However, one-way ANOVA and Tukey

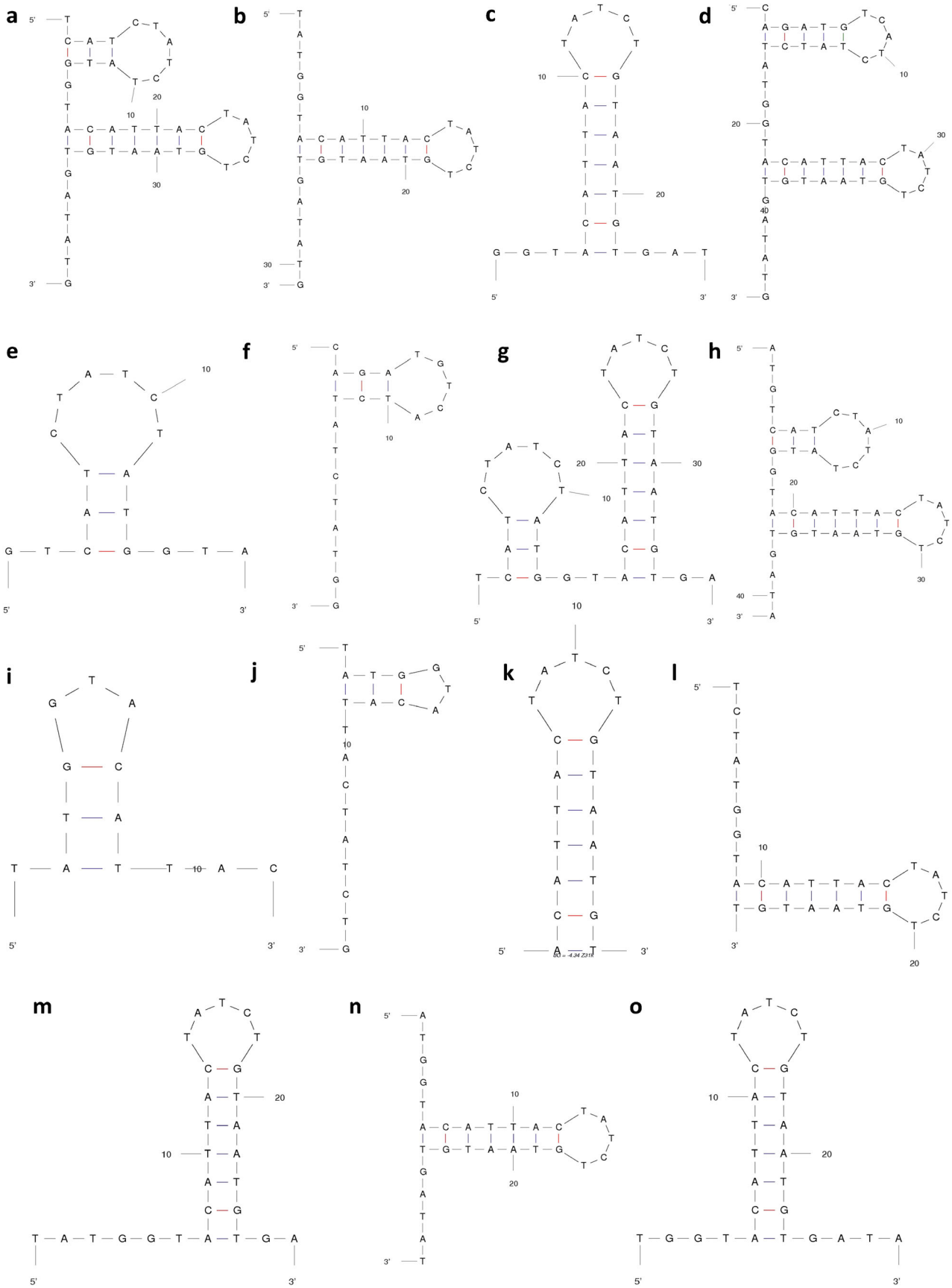

Fig. 2 New secondary structure of truncated aptamers predicted by Mfold software

Table 1 Truncated variants of ZEA aptamer with various bases length and lowest free energy

Aptamer ID	Sequence	Lowest free energy, ΔG (kcal/mol)
Z31A	TCATCTATCTATGGTACATTACTATCTGTAATGTGATATG	− 5.40
Z31B	TATGGTACATTACTATCTGTAATGTGATATG	− 5.55
Z31C	GGTACATTACTATCTGTAATGTGAT	− 5.55
Z31D	CAGATGTCATCTATCTATGGTACATTACTATCTGTAATGTGATATG	− 6.33
Z31E	GTCATCTATCTATGGTA	0.15
Z31F	CAGATGTCATCTATCTATGG	− 0.76
Z31G	TCATCTATCTATGGTACATTACTATCTGTAATGTGA	− 5.40
Z31H	ATGTCATCTATCTATGGTACATTACTATCTGTAATGTGATA	− 5.40
Z31I	TATGGTACATTAC	− 1.78
Z31J	TATGGTACATTACTATCTG	− 1.78
Z31K	ACATTACTATCTGTAATGT	− 4.34
Z31L	TCTATGGTACATTACTATCTGTAATGT	− 5.05
Z31M	TATGGTACATTACTATCTGTAATGTGA	− 5.55
Z31N	ATGGTACATTACTATCTGTAATGTGATAT	− 5.55
Z31O	TGGTACATTACTATCTGTAATGTGATA	− 5.55

HSD statistical test were done to evaluate the difference of Vina score between each aptamer, and the results were included in Table 2. The result of p value was compared to Z31A, which referred to the truncated 40-mer aptamer. Five truncated variants, including Z31B, Z31G, Z31L, Z31N, and Z31O, had lower free binding energy which were above − 7.0 kcal/mol. However, excluding Z31L, all 4 variants were significantly different from Z31A ($p < 0.05$). These five sequences were further aligned to determine the order or similarity of their base. As shown in Fig. 3, these 5 variants shared a similar bases order of 'TGGTACATTACTATCTGTAATGT', which strongly suggests that this section may be responsible for the binding event.

From a fundamental point of view, such predictions were an initial assessment of the physicochemical models on which they were based, including the underlying representation of the molecular interactions and conformational ensembles [30]. The conformational analysis of docked structures by PLIP showed that all aptamers bind to the specific locus in the ZEA epitope and formed hydrogen bonds with the specific aptamer binder residues in addition to the intramolecular hydrophobic interactions. At least two active binding residues

Table 2 Vina score of the predicted docking of truncated ZEA aptamer towards ZEA and the possible intermolecular interactions

Aptamer ID	Length	Vina score (kcal/mol)	Hydrophobic interactions	Hydrogen bonds	Salt bridges	π-Cation interactions	π-Stacking	p value
Z31A	40-mer	− 6.5	1	13	1	–	–	–
Z31B	31-mer	− 7.3	1	8	4	–	–	0.003*
Z31C	25-mer	− 6.4	2	12	2	–	–	1.000
Z31D	46-mer	− 6.8	1	9	2	–	–	0.707
Z31E	17-mer	− 5.8	–	7	1	1	–	0.009*
Z31F	20-mer	− 5.7	2	8	2	–	–	0.003*
Z31G	36-mer	− 7.1	2	12	4	–	–	0.032
Z31H	41-mer	− 6.9	3	11	2	1	1	0.324
Z31I	13-mer	− 5.4	–	9	–	1	–	0.000*
Z31J	19-mer	− 4.8	–	8	1	–	–	0.707
Z31K	19-mer	− 6.2	1	9	–	–	–	0.707
Z31L	27-mer	− 7.0	1	8	3	–	–	0.110
Z31M	27-mer	− 6.5	2	4	4	2	–	1.000
Z31N	29-mer	− 7.8	–	12	3	–	–	0.000*
Z31O	27-mer	− 7.2	2	8	3	–	–	0.009*

*Represents p value less than 0.05

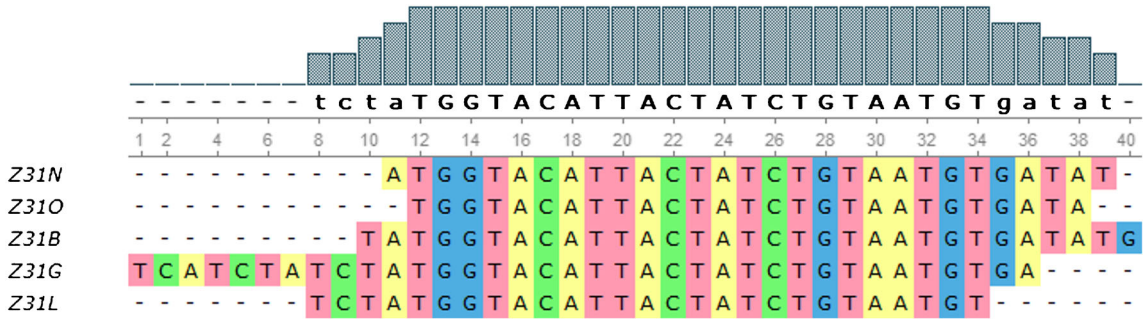

Fig. 3 Similarities of bases order of the top five truncated aptamers which had the lowest free binding energies by multiple sequence alignment

that functioned as the hydrogen donors towards aptamer were observed from almost all of the aptamer docking. These residues were responsible for maintaining the aptamer's position in docking. Nucleotide in aptamers has the ability to form salt bridges and hydrogen bonds with the receptor to maintain the dynamical interactions between two molecules [32]. Therefore, although the aptamers were moving during the binding, these bonds were holding the aptamer in place, thus affecting its affinity. The number of dynamic hydrogen bonds formed between ZEA and each truncated aptamer is shown in Table 2. Z31A, Z31C, Z31G, Z31H, and Z31N have more than 10 hydrogen bonds, with Z31G and Z31N having the highest number of the salt bridge. The intermolecular hydrogen bond occupancy could be considered as a benchmark in determining the active binding residues [32].

Conformational evaluation of aptamer by circular dichroism

Five out of fifteen truncated aptamers with the lowest binding energy predicted by the computational software were further evaluated using CD. The chosen aptamers include Z31B, Z31G, Z31L, Z31N, and Z31O. The conformational changes of these aptamers, if any, as a result of truncation, were studied. The aptamers were tested in the free and induced target-bounded form of ZEA in solution, as illustrated by the CD spectra in Fig. 4. All aptamers showed a negative peak at ~ 250 nm and a positive peak at ~ 275 nm, which indicated that B-form helix or hairpin structures primarily existed in the unbound aptamer's solution. These spectra were consistent with the previous predicted secondary structures that evaluate the hairpin structure of each truncated variants. From the results, the peaks have about the same intensity, and the integral of the spectral curves was closed to zero. This situation was known as spectrum conservative, which the base pairs were less perpendicular to the long axis of the double helix indicating a comparatively weak chirality into the structure [33].

After ZEA binding, the truncated aptamer variants of Z31B, Z31G, and Z31O showed similar features. An increase of the ellipticity at 275 and 250 nm of the aptamer was observed for aptamer Z31B (Fig. 4a), Z31G (Fig. 4b), and Z31O (Fig. 4e), which indicated folding of the aptamer into a different conformation. However, it could be observed that there was a slight shift of the peak for Z31L (Fig. 4c) and a significant shift in Z31N (Fig. 4d). These results confirmed that the target analyte induced a conformational change of the aptamer and further demonstrated their sensing ability. The CD spectra of truncated variant Z31N supported the work of predicted binding affinity by computational approach in Table 2, which showed that this truncated aptamer had the lowest Vina score with numbers of hydrogen bonds. It can therefore be assumed that the truncated variant of Z31N was the most effective truncated variant in targeting ZEA.

Visualisation of the aptamer-ZEA docking

The docking results from the AutoDock Vina were further visualised using PyMol software. Based on the results of the Vina score, evaluation of intermolecular forces by PLIP, and observation of conformational change by CD, a truncated variant of Z31N was chosen as the best truncated aptamer. Figure 5 shows the 3D structure of the aptamer Z31N-ZEA complex predicted binding mode. The accessible surface area (ASA) structure in red represents the Z31N aptamer while the blue molecule is ZEA analyte. It can be observed from the structure that ZEA and the aptamer were perfectly docked to each other.

Dissociation constant (K_d) determination of truncated aptamer using electrochemical impedance spectroscopy

The binding affinity of the selected truncated aptamer (Z31N) towards its target was further evaluated by electrochemical binding assay. A constant amount of ZEA was immobilised onto the electrode, and different concentrations of aptamer (ranging from 0 to 250 nM) were used to estimate the K_d. The Nyquist plots in Fig. 6a show that the semicircles were gradually increased with the increasing concentration of the aptamer, indicating the increment of charge transfer resistance (R_{CT}). This was attributed to more binding of the aptamer to the ZEA on the electrode leading to higher negatively charged DNA shielded on the surface. As shown in Fig. 6b, the K_d was

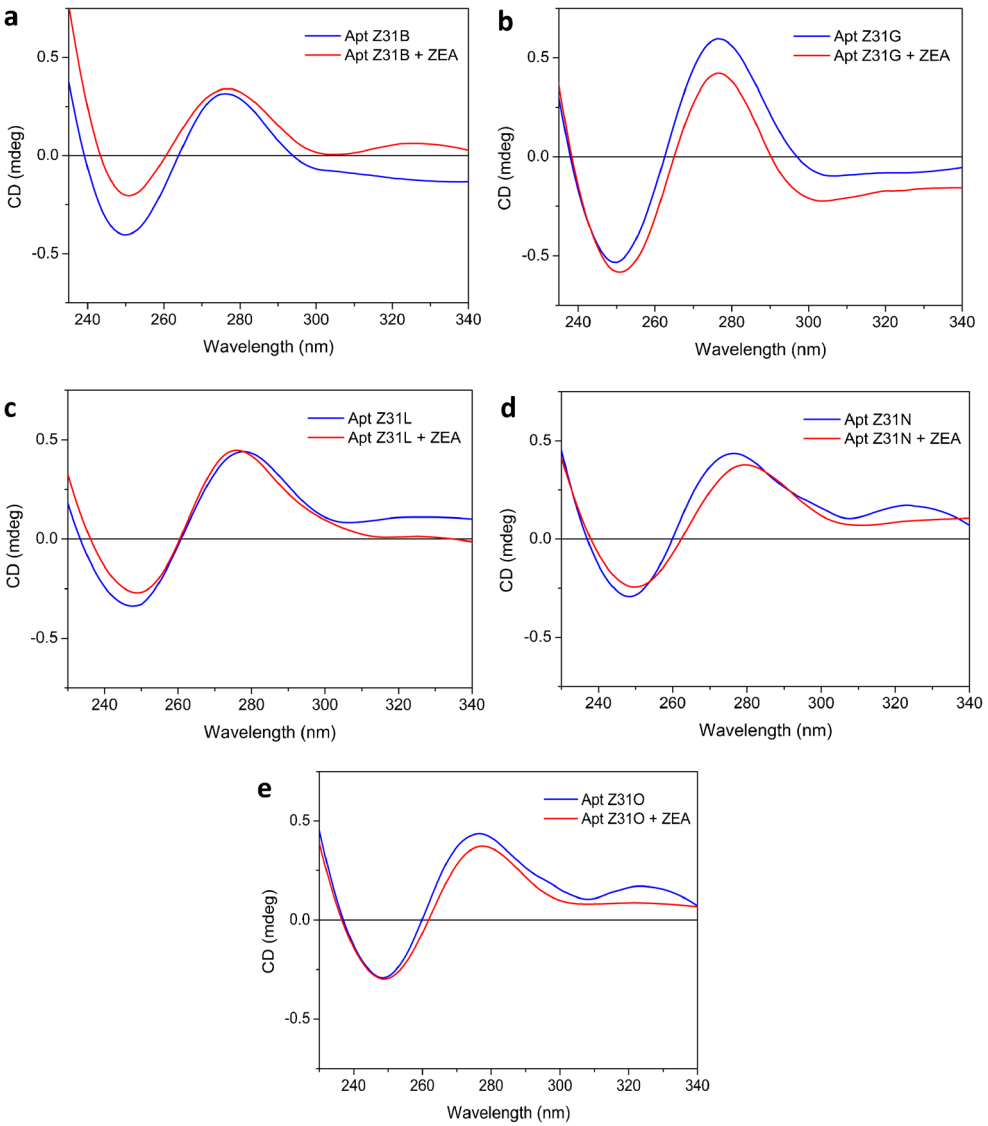

Fig. 4 Circular dichroism spectra of truncated variants **a** Z31B, **b** Z31G, **c** Z31L, **d** Z31N, and **e** Z31O in the presence of ZEA

then calculated using non-linear regression analysis by plotting the percentage change of the R_{CT} [$(R-R_0)/R_0\%$] vs. the aptamer concentration (nM). From the binding curve, the K_d of the truncated aptamer was calculated to be 11.77 ± 1.44 nM. These results supported that the truncation of the aptamer into shorter sequence improved the binding affinity of the aptamer, compared to the original aptamer, 41 nM (measured by magnetic bead-based UV-vis, [24]) or 30.8 ± 7 nM (measured by EIS, Fig. S2 in ESM).

Electrochemical detection of ZEA using truncated aptamer

The truncated aptamer of Z31N was further evaluated using the previously developed indirect competitive format to confirm the feasibility of the Z31N aptamer in detecting ZEA [10]. By employing a similar approach, the detection of ZEA in solutions was done with increasing ZEA concentrations from 0.0001 (0.314 pM) to 1000 ng/mL (3.14 nM). The competition occurred between the immobilised ZEA and the free ZEA for a binding site of a fixed amount of aptamer (50 nM). The electrochemical detection was performed using the SWV technique, and the signal was analysed based on the $(i_0-i)/i_0\%$ signal. As shown in Fig. 7a, the current increased with the increase of free ZEA concentration in the solution. This was due to the limited amount of aptamer available for binding to the immobilised ZEA on the gold electrode surface, which subsequently reduced the presence of the negatively charged aptamer onto the electrode surface. Therefore, with a higher concentration of the analyte, lower change in the sensor response $(i_0-i)/i_0\%$ was obtained.

A linear calibration plot is shown in Fig. 7b by plotting the analytical response, $(i_0-i)/i_0\%$ signal vs. ZEA concentration (ng/mL). The linear plot has a negative slope, which indicated that the sensor response signal decreased as the ZEA concentration increased. The calibration plot was fitted to a linear equation ($y = mx + c$), where y is the $(i_0-i)/i_0\%$ signal, m is

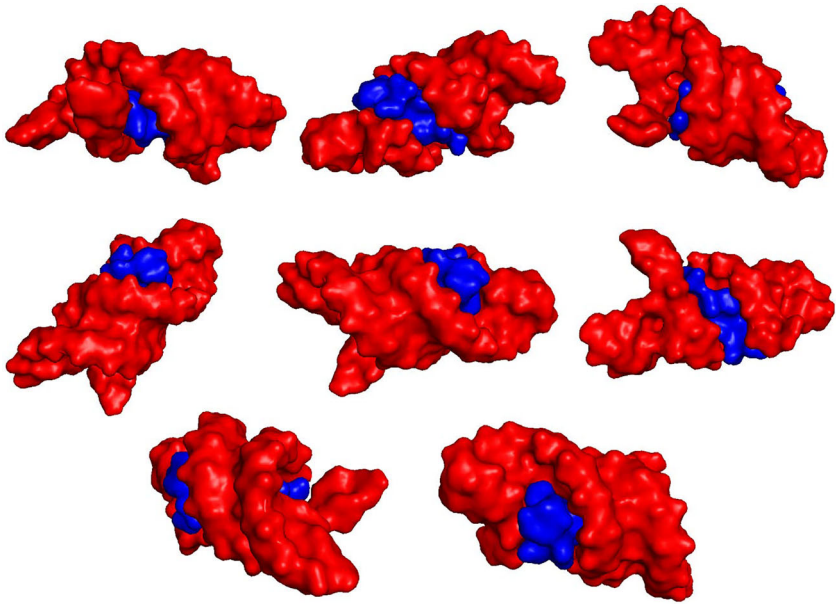

Fig. 5 Three-dimensional configuration of aptamer-analyte complex molecules. The images were captured by rotating the complex molecule at 360°. The red molecule represents Z31N truncated aptamer, while the blue molecule is ZEA

the slope of the gradient, and c is the y-intercept. The linear range obtained was in the range of 0.001 to 100 ng/mL. The best-fit values of the experimental data were $y = -4.77x + 36.72$, with a coefficient of determination, $R^2 = 0.989$. The limit of detection (LOD) was calculated as 3 × SD of the blank/slope to be 1.5 pg/mL (47 pM). Thus, the results confirmed that the Z31N aptamer enable to detect ZEA with an enhanced sensitivity.

Conclusion

The ability of the computational docking program for prediction of ligand-nucleic acid complexes was successfully examined in this study. This technique provides a simple, cheap, and easy to perform without the need of doing wet laboratory works. Computational docking is important in understanding the complex binding orientation with the lowest binding energy. The intermolecular interaction results also provide an insight on the tightness of aptamer-protein binding complex. Truncation by eliminating the non-binding regions and predicted free energy by computational docking simulation revealed that the right hairpin loop was involved in binding. In addition, the experimental study in determination of binding affinity by EIS confirmed that the affinity of the aptamer was significantly increased, compared to the 80-mer. The feasibility of the truncated aptamer was further evaluated by implementation in an indirect competitive electrochemical aptasensor and demonstrated that the truncated aptamer leads to an enhancement of the sensitivity of the biosensor.

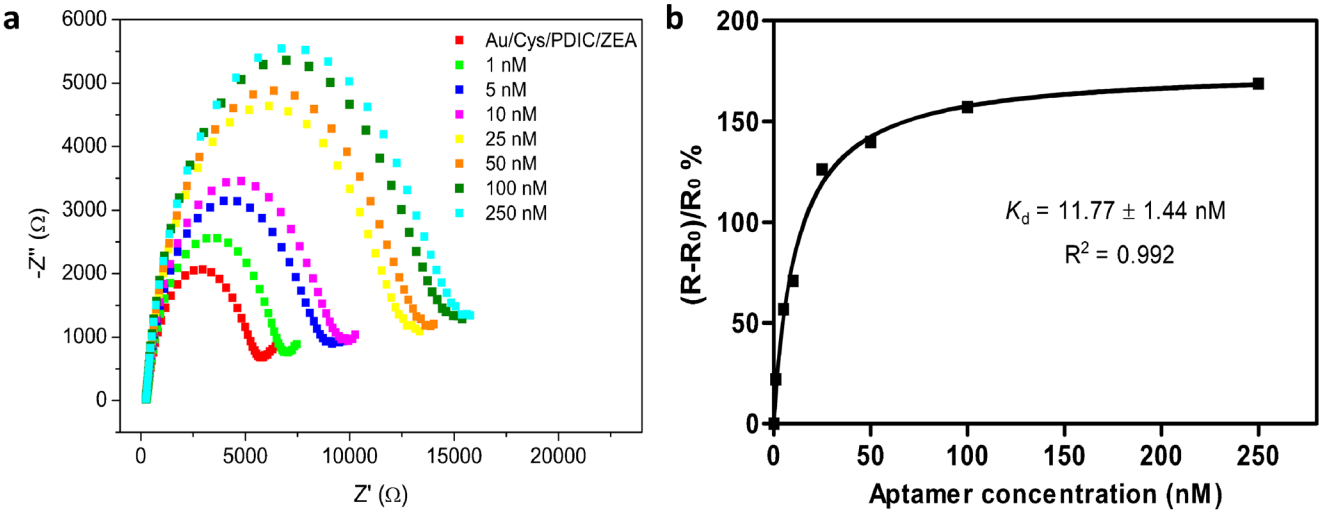

Fig. 6 **a** Nyquist plots of the ZEA electrode before and after incubation with different concentrations of Z31N aptamer and **b** non-linear regression plot of $(R-R_0)/R_0$% signal of the binding vs. aptamer concentration (nM) which represents the binding affinity of the aptamer

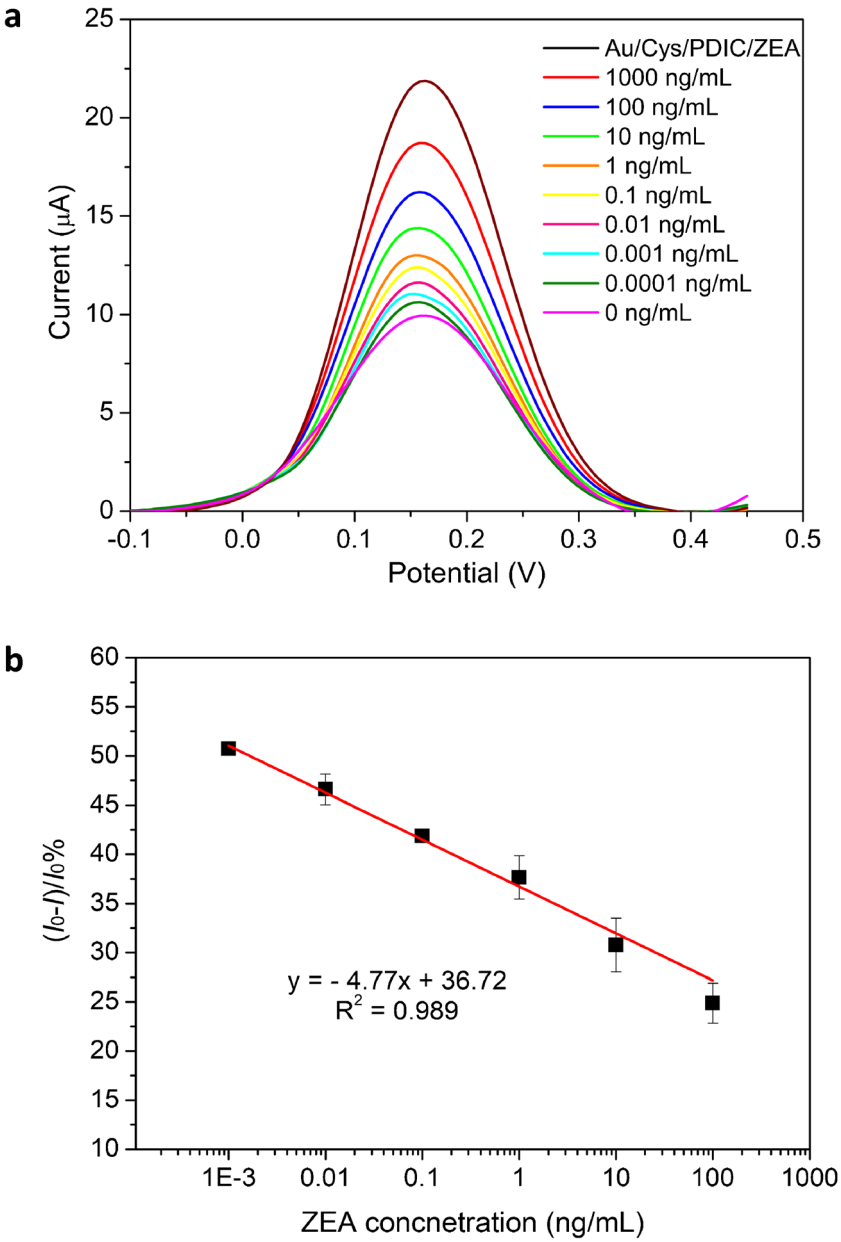

Fig. 7 Electrochemical detection of ZEA based on indirect competitive format. **a** SWV signals of the fabricated electrode after incubation with 50 nM aptamer and **b** calibration plot based on the $(i_0-i)/i_0\%$ signal vs. log concentration of ZEA. Data are presented as mean ± SD of duplicate measurements ($n = 2$)

Supplementary Information The online version contains supplementary material available at https://doi.org/10.1007/s00216-021-03336-1.

Funding This work was supported by the Malaysian Ministry of Higher Education under the High Impact Centre of Excellence (HICoE) grant scheme (HICoE/ITAFOS/2017/FS9) and Universiti Putra Malaysia for providing Graduate Research Fellowship (GRF).

Declarations

Conflict of interest The authors declare no competing interests.

References

1. Ruscito A, DeRosa MC. Small-molecule binding aptamers: selection strategies, characterization, and applications. Front Chem. 2016;4:1–14. https://doi.org/10.3389/fchem.2016.00014.
2. Al Rubaye A, Nabok A, Catanante G, Marty J, Takacs E, Szekacs A. Detection of ochratoxin A in aptamer assay using total internal reflection ellipsometry. Sensors Actuators B Chem. 2018;263:248–51. https://doi.org/10.1016/j.snb.2018.01.220.
3. Myndrul V, Viter R, Savchuk M, Shpyka N, Erts D. Porous silicon based photoluminescence immunosensor for rapid and highly-sensitive detection of ochratoxin A. Biosens Bioelectron. 2017;102:661–7. https://doi.org/10.1016/j.bios.2017.11.048.

4. Shim W, Jin M, Mun H, Kim M. An aptamer-based dipstick assay for the rapid and simple detection of aflatoxin B1. Biosens Bioelectron. 2014;62:288–94. https://doi.org/10.1016/j.bios.2014.06.059.
5. Yang X, Qian J, Jiang L, Yan Y, Wang K, Liu Q, et al. Ultrasensitive electrochemical aptasensor for ochratoxin A based on two-level cascaded signal amplification strategy. Bioelectrochemistry. 2014;96:7–13. https://doi.org/10.1016/j.bioelechem.2013.11.006.
6. Al-Jawdah A, Nabok A, Abu-Ali H, Catanante G, Marty JL, Szekacs A. Highly sensitive label-free in vitro detection of aflatoxin B1 in an aptamer assay using optical planar waveguide operating as a polarization interferometer. Anal Bioanal Chem. 2019;411:7717–24. https://doi.org/10.1007/s00216-019-02033-4.
7. Wang C, Li Y, Zhou C, Zhao Q. Fluorometric determination of aflatoxin B1 using a labeled aptamer and gold nanoparticles modified with a complementary sequence acting as a quencher. Microchim Acta. 2019;186:1–5. https://doi.org/10.1007/s00604-019-3838-2.
8. Wei M, Xin L, Feng S, Liu Y. Simultaneous electrochemical determination of ochratoxin A and fumonisin B1 with an aptasensor based on the use of a Y-shaped DNA structure on gold nanorods. Microchim Acta. 2020;187:1–7. https://doi.org/10.1007/s00604-019-4089-y.
9. Tao Z, Zhou Y, Li X, Wang Z. Competitive HRP-linked colorimetric aptasensor for the detection of fumonisin B1 in food based on dual biotin-streptavidin interaction. Biosensors. 2020;10:1–11. https://doi.org/10.3390/bios10040031.
10. Azri FA, Eissa S, Zourob M, Chinnappan R, Sukor R, Yusof NA, et al. Electrochemical determination of zearalenone using a label-free competitive aptasensor. Microchim Acta. 2020;87:1–10. https://doi.org/10.1007/s00604-020-4218-7.
11. Ma L, Bai L, Zhao M, Zhou J, Chen Y, Mu Z. An electrochemical aptasensor for highly sensitive detection of zearalenone based on PEI-MoS 2 -MWCNTs nanocomposite for signal enhancement. Anal Chim Acta. 2019;1060:71–8. https://doi.org/10.1016/j.aca.2019.02.012.
12. He B, Yan X. An amperometric zearalenone aptasensor based on signal amplification by using a composite prepared from porous platinum nanotubes, gold nanoparticles and thionine-labelled graphene oxide. Microchim Acta. 2019;186:383–92.
13. He B, Yan X. Ultrasensitive electrochemical aptasensor based on CoSe2/AuNRs and 3D structured DNA-PtNi@Co-MOF networks for the detection of zearalenone. Sensors Actuators B Chem. 2020;306:127558. https://doi.org/10.1016/j.snb.2019.127558.
14. Nuryono N, Noviandi CT, Bohm J, Razzazi-Fazeli E. A limited survey of zearalenone in Indonesian maize-based food and feed by ELISA and high performance liquid chromatography. Food Control. 2005;16:65–71. https://doi.org/10.1016/j.foodcont.2003.11.009.
15. Lönne M, Zhu G, Stahl F, Walter JG. Aptamer-modified nanoparticles as biosensors. In: Gu MB, Kim HS, editors. Biosensors based on aptamers and enzymes. Verlag Berlin Heidelberg: Springer; 2014. p. 120–54.
16. Le TT, Chumphukam O, Cass AEG. Determination of minimal sequence for binding of an aptamer. A comparison of truncation and hybridization inhibition methods. RSC Adv. 2014;4:47227–33. https://doi.org/10.1039/c4ra08243e.
17. O'Sullivan CK. Aptasensors–the future of biosensing? Anal Bioanal Chem. 2002;372:44–8. https://doi.org/10.1007/s00216-001-1189-3.
18. Alhadrami HA, Chinnappan R, Eissa S, Rahamn AA, Zourob M. High affinity truncated DNA aptamers for the development of fluorescence based progesterone biosensors. Anal Biochem. 2017;525:78–84. https://doi.org/10.1016/j.ab.2017.02.014.
19. Almusharraf AY, Eissa S, Zourob M. Truncated aptamers for total and glycated hemoglobin, and their integration into a graphene oxide-based fluorometric method for high-throughput screening for diabetes. Microchim Acta. 2018;185:1–8. https://doi.org/10.1007/s00604-018-2789-3.
20. Gao S, Zheng X, Jiao B, Wang L. Post-SELEX optimization of aptamers. Anal Bioanal Chem. 2016;408:4567–73. https://doi.org/10.1007/s00216-016-9556-2.
21. Alonso H, Bliznyuk AA, Gready JE. Combining docking and molecular dynamic simulations in drug design. Med Res Rev. 2006;26:531–68. https://doi.org/10.1002/med.20067.
22. Bhakat S, Åberg E, Söderhjelm P. Prediction of binding poses to FXR using multi-targeted docking combined with molecular dynamics and enhanced sampling. J Comput Aided Mol Des. 2018;32:59–73. https://doi.org/10.1007/s10822-017-0074-x.
23. Nnyigide OS, Lee SG, Hyun K. In silico characterization of the binding modes of surfactants with bovine serum albumin. Sci Rep. 2019;9:1–16. https://doi.org/10.1038/s41598-019-47135-2.
24. Chen X, Huang Y, Duan N, Wu S, Ma X, Xia Y, et al. Selection and identification of ssDNA aptamers recognizing zearalenone. Anal Bioanal Chem. 2013:6573–81. https://doi.org/10.1007/s00216-013-7085-9.
25. Dhiman A, Kalra P, Bansal V, Bruno JG, Sharma TK. Aptamer-based point-of-care diagnostic platforms. Sensors Actuators B Chem. 2017;246:535–53. https://doi.org/10.1016/j.snb.2017.02.060.
26. Rockey WM, Hernandez FJ, Huang SY, Cao S, Howell CA, Thomas GS, et al. Rational truncation of an RNA aptamer to prostate-specific membrane antigen using computational structural modeling. Nucleic Acid Ther. 2011;21:299–314. https://doi.org/10.1089/nat.2011.0313.
27. Djordjevic M. SELEX experiments: new prospects, applications and data analysis in inferring regulatory pathways. Biomol Eng. 2007;24:179–89. https://doi.org/10.1016/j.bioeng.2007.03.001.
28. Kypr J, Kejnovská I, Bednářová K, Vorlíčková M. Circular dichroism spectroscopy of nucleic acids. Compr Chiroptical Spectrosc. 2012;2:575–86. https://doi.org/10.1002/9781118120392.ch17.
29. Dong Y, Wang S. Enzyme-linked aptamer assay (ELAA). In: Dong Y, editor. Aptamers for analytical applications. Beijing: Wiley VCH; 2018. p. 219–27.
30. Foloppe N, Hubbard R. Towards predictive ligand design with free-energy based computational methods. Curr Med Chem. 2006;13:3583–608. https://doi.org/10.2174/092986706779026165.
31. Du X, Li Y, Xia YL, Ai SM, Liang J, Sang P, et al. Insights into protein–ligand interactions: mechanisms, models, and methods. Int J Mol Sci. 2016;17:1–34. https://doi.org/10.3390/ijms17020144.
32. Sabri MZ, Abdul Hamid AA, Sayed Hitam SM, Abdul Rahim MZ. In silico screening of aptamers configuration against hepatitis B surface antigen. Adv Bioinforma. 2019;2019:1–12. https://doi.org/10.1155/2019/6912914.
33. Kypr J, Kejnovská I, Bednářová K, Vorlíčková M. Circular dichroism of protein-nucleic acid interactions. In: Berova N, Polavarapu PL, Nakanishi K, Woody RW, editors. Comprehensive chiroptical spectroscopy. New Jersey: Wiley; 2012. p. 615–33.